Enhanced photon antibunching via interference effects in a Δ configuration

Jiahua Li,[1,*] Chunling Ding,[2,†] and Ying Wu[1,‡]
[1]*School of Physics, Huazhong University of Science and Technology, Wuhan 430074, People's Republic of China*
[2]*Hubei Key Laboratory of Optical Information and Pattern Recognition, Wuhan Institute of Technology, Wuhan 430205, People's Republic of China*

(Received 24 March 2019; published 12 September 2019)

Photon antibunching based on a single two-level atom strongly coupled to a single-mode optical cavity has been demonstrated in experiments. Here, we put forward an improved version of such an antibunching by introducing a pump field and a microwave field in the coupled atom-cavity system to form both a three-level Δ-type transition and closed-loop coupling. Via calculating the zero-time-delay second-order correlation function $g^{(2)}(0)$ of the single-mode cavity field, we find that a complete photon blockade, namely, $g^{(2)}(0) = 0$, can be well achieved without detuning the driving and cavity resonance. In addition, it is clearly shown that this strong photon antibunching effect appears in the weak-coupling regime of light-atom interactions. The enhanced photon antibunching is ascribed to quantum interference between the two transition paths from the three-level Δ atom weakly coupled to the three involved fields (cavity, pump, and microwave). Our proposal is useful for the single-photon generation by photon blockade, which has applications in quantum information processing.

DOI: 10.1103/PhysRevA.100.033814

I. INTRODUCTION

A two-level quantum emitter coupled to a single-mode optical cavity belonging to cavity quantum electrodynamics (QED) displays many notable quantum behaviors. As is well known, in the weak-coupling regime of cavity QED where the coupling strength between the emitter and the cavity mode is much less than the dissipative rate, an enhancement of the spontaneous emission rate, namely, the so-called Purcell effect, can appear [1] and in experiment has been observed [2]. By contrast, in the strong-coupling regime, the energy eigenvalues and eigenstates of the cavity-QED system are considerably varied, which leads to hybridized polaritons (dressed state), Rabi oscillation [3], and Rabi splitting [4,5]. Accordingly, the energy-level diagram of the full system is described by the anharmonic Jaynes-Cummings (JC) ladder [6–10]. Thanks to the anharmonic energy-level spacing, when the driving field is positioned at one of the two energy eigenstates corresponding to the vacuum Rabi splitting, the admission of a single photon into the cavity diminishes the probability for a second photon to enter the cavity. This phenomenon is called photon antibunching [11,12]. Whereas when the driving field is positioned between the two eigenstates, the probability of capturing subsequent photons is raised, resulting in photon bunching. In the strong-coupling regime of cavity QED or circuit QED, photon antibunching has been illustrated in one trapped atom in a Fabry-Pérot or whispering-gallery cavity [13–16], an embedded quantum dot in a photonic crystal or micropillar cavity [17–24], and a superconducting qubit in a superconducting circuit resonator [25–27], spinning or gain resonator [28,29].

However, it is noteworthy to mention that, in the weak-coupling scenario, the photon antibunching in the above-mentioned cavity QED is impossible because the energy gap between the hybridized polaritonic states disappears. Again, arriving at the strong-coupling regime in the optical domain is a highly challenging task. As a consequence, it is still of fundamental and practical interest to seek novel mechanisms to produce the strong antibunched light in the weak-coupling regime, which is much easier to achieve.

With this motivation, in 2010 Liew and Savona theoretically found that the constraint condition on the strong coupling can be relaxed by taking into account two coupled cavities rather than one single cavity [30] for generating perfect photon antibunching $g^{(2)}(0) = 0$. This effect is referred to as an unconventional photon blockade because the underlying mechanism behind it is based on the destructive quantum interference between multiple transition pathways in two directly coupled cavities [31] or is based on the fact that the cavity state is a displaced squeezed state [32], with respect to conventional photon blockade from anharmonicity of the JC ladder of eigenstates [13,17,18]. From then on, all kinds of theoretical methods based on such a physical mechanism have been proposed to achieve the antibunched light, for instance, in a bimodal cavity or two cavities coupling a dipole quantum emitter [33–39], in two directly coupled single-mode cavities with second-order or third-order optical nonlinearity [40–48], in coupled cavity optomechanical systems [49–53], and in coupled polaritonic systems [54–56], due to its potential applications in quantum communication and quantum information processing. After considerable efforts, in 2018 the unconventional photon blockade has been experimentally implemented and demonstrated by two independent groups. One group used a single quantum dot and a micropillar cavity with two orthogonally polarized modes, which functions like two cavities [57]. At the same time, the other group adopted two coupled superconducting circuit resonators, where one

*huajia_li@126.com
†clding2006@126.com
‡yingwu2@126.com

resonator contains a superconducting quantum interference device [58].

On the other hand, coherently driven three-level atoms or comparable solid-state emitters instead of two-level atoms inside an optical cavity are exploited to study a variety of new quantum optical phenomena because the absorption, dispersion, and nonlinearity of the three-level atomic system based on quantum coherence and interference can be drastically modified [59–66]. Along this line, in the present work we investigate the quality of the photon antibunching, namely, the smallness of the second-order intensity correlation function at zero time, using a single three-level atom embedded in a single-mode optical cavity together with a pump field and a microwave field in free space. In this scenario, the involved three fields and three-level atom can form the so-called Δ-type transition and closed-loop coupling. Based on experimentally realistic atom-cavity parameters, we numerically calculate the steady-state second-order intensity correlation functions $g^{(2)}(0)$ of the cavity field for four geometries: (i) a two-level configuration, (ii) a three-level Λ configuration, (iii) a three-level V configuration, and (iv) a three-level Δ configuration for the purpose of a performance comparison. The detailed results clearly display that the quality of the photon antibunching in the three-level Δ configuration can be significantly improved, as compared to the other three configurations. The complete photon blockade [i.e., $g^{(2)}(0) = 0$] can be generated at the zero driving detuning. The photon antibunching behavior in this three-level Δ configuration does not directly arise from the anharmonicity mechanism as in the previous studies [13–16] and also is distinct from the cavity-cavity coupling principle of the unconventional photon blockade in previously implemented proposals [30,31]. Here the photon statistics of the cavity field is influenced by the external field couplings (for example, the pump and microwave fields in free space in the present scheme) and is determined by the whole interacting dynamical process of the system which needs to include the photon-photon correlation induced by the intermediary JC interactions.

On the other hand, this strong photon antibunching effect can appear in the weak-coupling regime of light-atom interactions, where the coupling strength between the atom and the field is much less than the cavity or atom decay rate. This relaxes the constraint condition on the considered system and makes our proposal well suited to generate the antibunched photons, as we show below. We attribute these striking features to the formation of the quantum interference between the two relevant transition paths from the three-level Δ-type atom weakly coupled to the cavity, pump, and microwave fields (see inset of Fig. 1). We also explore the experimental feasibility of the proposed scheme using current state-of-the-art atom-cavity architecture. This investigation deepens our understanding of the photon antibunching mechanism in the closed-loop coupling and may be useful for the construction of single-photon sources.

The outline of our paper is organized as follows. Section II details the basic framework of our three-level Δ-type atom-cavity system under study, which mainly includes the corresponding Hamiltonian and master equation. Section III discusses the experimental feasibility of our scheme. Section IV presents the in-depth results of the photon statistics for the cavity field. Finally, we summarize our conclusions in Sec. VI.

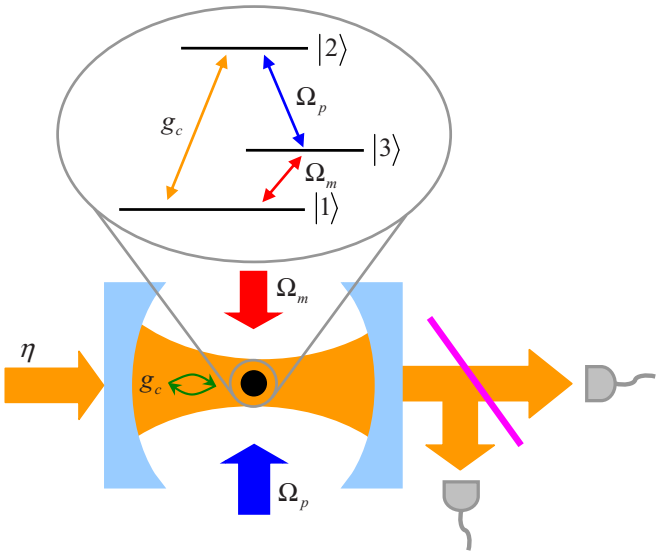

FIG. 1. Schematic representation of the system to generate antibunched photons. The medium is a single atom trapped at the center of a two-sided optical high-finesse cavity. The atom is modeled as a three-level system composed by an excited state $|2\rangle$ as well as two ground states $|1\rangle$ and $|3\rangle$ which are separated by a microwave transition shown in the inset. The cavity mode with frequency ω_c and vacuum Rabi frequency g_c (orange lines) couples the dipole-allowed transition $|1\rangle \leftrightarrow |2\rangle$. The cavity mode is driven along the cavity axis by an external weak laser field with frequency ω_L and strength η. A classical pump laser field (free-space) with frequency ω_p and Rabi frequency Ω_p (blue lines) couples an optical electric-dipole transition $|2\rangle \leftrightarrow |3\rangle$. Simultaneously, an additional microwave field with frequency ω_m and Larmor frequency Ω_m (red lines) couples a magnetic dipole transition $|1\rangle \leftrightarrow |3\rangle$. The top inset shows the atomic level scheme. The cycle transition $|1\rangle \rightarrow |2\rangle \rightarrow |3\rangle \rightarrow |1\rangle$ together with the three fields (cavity, pump, and microwave) forms a so-called Δ atomic level configuration. The other parameters are defined in the text.

II. PHYSICAL SYSTEM AND THEORETICAL FRAMEWORK

As depicted schematically in Fig. 1, we consider a system consisting of a three-level atom characterized by an excited state $|2\rangle$ and two ground states $|1\rangle$ and $|3\rangle$ in a Δ configuration plus closed-loop coupling ($|1\rangle \overset{g_c}{\rightsquigarrow} |2\rangle \overset{\Omega_p}{\rightsquigarrow} |3\rangle \overset{\Omega_m}{\rightsquigarrow} |1\rangle$) and trapped inside a high-finesse single-mode optical cavity. The ground state $|1\rangle$ and the excited state $|2\rangle$ with the atomic transition frequency ω_{21} are coupled by the cavity mode with the resonance frequency ω_c and the atom-cavity coupling constant (vacuum Rabi frequency) g_c as described by cavity QED. This cavity mode is driven coherently by an external weak guided field with frequency ω_L and strength η. To change the optical properties of the atom, the states $|2\rangle$ and $|3\rangle$ with the transition frequency ω_{23} are coupled by a classical pump laser field in free space with angular frequency ω_p and Rabi frequency Ω_p. The two ground states $|1\rangle$ and $|3\rangle$, separated by a microwave transition with frequency ω_{31}, are coupled by a microwave

field with angular frequency ω_m and Larmor frequency Ω_m. In the dipole and rotating-wave approximations, the overall Hamiltonian of the composite system which describes the atom-field coupling can be written as

$$\begin{aligned}\hat{H} &= \hbar\omega_c\hat{a}_c^\dagger\hat{a}_c + \hbar\omega_{21}\hat{\sigma}_{22} + \hbar\omega_{31}\hat{\sigma}_{33} \\ &+ \hbar(g_c\hat{a}_c\hat{\sigma}_{21} + g_c^*\hat{a}_c^\dagger\hat{\sigma}_{12}) \\ &+ \hbar(\Omega_p e^{-i\omega_p t}\hat{\sigma}_{23} + \Omega_p^* e^{i\omega_p t}\hat{\sigma}_{32}) \\ &+ \hbar(\Omega_m e^{-i\omega_m t}\hat{\sigma}_{31} + \Omega_m^* e^{i\omega_m t}\hat{\sigma}_{13}) \\ &+ \hbar(\eta e^{-i\omega_L t}\hat{a}_c^\dagger + \eta^* e^{i\omega_L t}\hat{a}_c). \end{aligned} \tag{1}$$

Here, $\hbar$ is the reduced Planck constant and $\hat{\sigma}_{ij} = |i\rangle\langle j|$ ($i, j = 1, 2, 3$) are the atomic energy-level population operators ($i = j$) and the atomic raising and lowering operators ($i \neq j$); $\hat{a}_c^\dagger$ and $\hat{a}_c$ are the creation and annihilation operators for photons inside the cavity obeying the bosonic commutation rule $[\hat{a}_c, \hat{a}_c^\dagger] = 1$, $[\hat{a}_c, \hat{a}_c] = 0$, and $[\hat{a}_c^\dagger, \hat{a}_c^\dagger] = 0$, respectively. The corresponding Rabi and Larmor frequencies are defined as $g_c = \mu_{21}\sqrt{\omega_c/2\hbar\varepsilon_0 V}$, $\Omega_p = \mu_{23}E_p/2\hbar$, and $\Omega_m = \mu_{31}E_m/2\hbar$ with ε_0 being the permittivity of vacuum, V the mode volume of the cavity, μ_{ij} the dipole moment of the corresponding transition, and E_p and E_m the field amplitudes. Notice that our definition of Ω_p (Ω_m) corresponds to half of the standard definition of Rabi (Larmor) frequency.

We utilize a rotating coordinate frame described by the unitary operator $\hat{U} = e^{-i\hat{H}_0 t/\hbar}$, where

$$\hat{H}_0 = \hbar\omega_L\hat{a}_c^\dagger\hat{a}_c + \hbar\omega_L\hat{\sigma}_{22} + \hbar(\omega_L - \omega_d)\hat{\sigma}_{33}. \tag{2}$$

Then, making good use of the formula $\hat{H}_{rot} = \hat{U}^\dagger\hat{H}\hat{U} - i\hat{U}^\dagger\partial\hat{U}/\partial t$, Hamiltonian (1) can be transformed into a time-independent form

$$\begin{aligned}\hat{H}_{\rm rot} &= \hbar\delta\hat{a}_c^\dagger\hat{a}_c + \hbar(\delta + \Delta_c)\hat{\sigma}_{22} + \hbar(\delta + \Delta_c - \Delta_p)\hat{\sigma}_{33} \\ &+ \hbar(g_c\hat{a}_c\hat{\sigma}_{21} + g_c^*\hat{a}_c^\dagger\hat{\sigma}_{12}) + \hbar(\Omega_p\hat{\sigma}_{23} + \Omega_p^*\hat{\sigma}_{32}) \\ &+ \hbar(\Omega_m\hat{\sigma}_{31} + \Omega_m^*\hat{\sigma}_{13}) + \hbar(\eta\hat{a}_c^\dagger + \eta^*\hat{a}_c), \end{aligned} \tag{3}$$

where we have introduced the notations of frequency detunings $\delta = \omega_c - \omega_L$, $\Delta_c = \omega_{21} - \omega_c$, $\Delta_p = \omega_{23} - \omega_p$, and $\Delta_m = \omega_{31} - \omega_m$ for the corresponding fields, respectively. All three fields are detuned from the respective resonances in the three-level atom, but they are in the three-photon resonance, $\omega_m + \omega_p = \omega_L$, which leads to the relationship $\Delta_m + \Delta_p = \Delta_c + \delta$.

To capture the dynamics of our physical system, we numerically solved the Markovian master equation of the driven system for the density matrix $\hat{\rho}$ in the Lindblad form [67]:

$$\begin{aligned}\frac{\partial\hat{\rho}}{\partial t} &= -\frac{i}{\hbar}[\hat{H}_{\rm rot}, \hat{\rho}] + \kappa_c(\bar{n}_{th} + 1)\mathcal{L}(\hat{a}_c) + \kappa_c\bar{n}_{th}\mathcal{L}(\hat{a}_c^\dagger) \\ &+ \gamma_{21}\mathcal{L}(\hat{\sigma}_{12}) + \gamma_{23}\mathcal{L}(\hat{\sigma}_{32}), \end{aligned} \tag{4}$$

where $\hat{H}_{\rm rot}$ is Hamiltonian (3) of the atom-cavity system and κ_c is the decay rate of the cavity field. γ_{21} and γ_{23} are the spontaneous decay rates of the atomic dipole from the common excited state $|2\rangle$ to the two ground states $|1\rangle$ and $|3\rangle$, respectively. $\bar{n}_{th}$ is the mean photon number of thermal excitations at the cavity frequency ω_c, i.e., $\bar{n}_{th} = (e^{\hbar\omega_c/k_B T} - 1)^{-1}$ with T being the bath temperature and k_B the Boltzmann constant. Here we assume a zero-temperature bath for the optical cavity, i.e., $T = 0$ K, thus giving rise to $\bar{n}_{th} = 0$. On the right-hand side of Eq. (4), the first term represents the coherent evolution of the system, while the other incoherent terms describe the damping phenomena, namely, the cavity field damping and the atomic spontaneous emission processes. These damping effects are expressed by the Liouville superoperator $\mathcal{L}$, which acts on a given operator $\hat{\mathcal{O}}$ with the form $\mathcal{L}(\hat{\mathcal{O}}) = \hat{\mathcal{O}}\hat{\rho}\hat{\mathcal{O}}^\dagger - \hat{\mathcal{O}}^\dagger\hat{\mathcal{O}}\hat{\rho}/2 - \hat{\rho}\hat{\mathcal{O}}^\dagger\hat{\mathcal{O}}/2$.

III. POSSIBLE EXPERIMENTAL REALIZATION IN THIS MODEL

Before proceeding, we briefly address the experimental feasibility of our scheme by means of a two-sided Fabry-Pérot cavity, a single alkali-metal atom, two separate external cavity diode lasers (ECDLs), and an appropriate microwave source. More specifically, we employ, for example, a single ^{87}Rb atom (nuclear spin $I = 3/2$, D_1 line, and wavelength 795 nm) on the $5S$-$5P$ transition as a possible candidate [68,69] for achieving the Δ configuration under study. The designated states and the decay rates in the inset of Fig. 1 can be chosen as follows: $|1\rangle = |5S_{1/2}, F = 1, m_F = -1\rangle$, $|2\rangle = |5P_{1/2}, F = 1, m_F = -1\rangle$, $|3\rangle = |5S_{1/2}, F = 2, m_F = -2\rangle$, and $\gamma_{21} = \gamma_{23} \simeq 2\pi \times 3$ MHz [70,71], respectively, where F represents the hyperfine state and m_F the Zeeman substate. It should be pointed out that the relaxation rate γ_{31} of coherence between states $|3\rangle$ and $|1\rangle$ is negligible ($\gamma_{31} \simeq 2\pi \times 0.003$ MHz) because this transition is electric-dipole forbidden in our considered model.

Before being trapped at the center of a high-finesse optical cavity, the ^{87}Rb atoms need to be cooled by the magneto-optical trap positioned above the cavity and transferred into the cavity. In recent years, optical control has been successfully realized in current state-of-the-art single-atom cavity-QED experiments, described in detail in Refs. [72–79]. The atom in states $|1\rangle = |5S_{1/2}, F = 1, m_F = -1\rangle$ and $|2\rangle = |5P_{1/2}, F = 1, m_F = -1\rangle$ can be coupled to the linearly polarized fundamental mode of the cavity. An external driving laser field coming from an ECDL and pumping the linearly polarized cavity mode is scanned across the resonance of the $|1\rangle = |5S_{1/2}, F = 1, m_F = -1\rangle \leftrightarrow |2\rangle = |5P_{1/2}, F = 1, m_F = -1\rangle$ transition. A right-circularly polarized pump laser field Ω_p in free space, whose wavelength is 795 nm and which is applied to the electric-dipole transition $|3\rangle = |5S_{1/2}, F = 2, m_F = -2\rangle \leftrightarrow |2\rangle = |5P_{1/2}, F = 1, m_F = -1\rangle$, can be obtained from the ECDL. A microwave field, which comes from a home-made antenna [80], drives the magnetic dipole transition between $|1\rangle = |5S_{1/2}, F = 1, m_F = -1\rangle$ and $|3\rangle = |5S_{1/2}, F = 2, m_F = -2\rangle$ with the hyperfine splitting frequency $\omega_{31} \simeq 6.84$ GHz. Such a microwave-field coupling has experimentally arrived at values of hundreds of kilohertz [80]. The frequency difference between the cavity mode and the pump laser is also locked to the frequency difference of 6.84 GHz.

For the calculation the cavity parameters are set as the atom-cavity coupling rate $g_c = 2\pi \times 4$ MHz and the cavity field decay rate $\kappa_c = 2\pi \times 8$ MHz. For the cavity length $L = 486\mu$m, its finesse is $\mathcal{F} = \pi c/(2\kappa_c L) \simeq 2 \times 10^4$ with c being the light speed in free space. These cavity parameter values are fairly representative of the generic experimental single-atom

cavity-QED conditions [72–79]. For our selected parameters above, the atom-cavity system operates in the weak-coupling regime owing to $g_c < (\kappa_c, \Gamma_2)$, where $\Gamma_2 = \gamma_{21} + \gamma_{23}$. Correspondingly, we have the cooperativity parameter of the system, $C = g_c^2/(2\kappa_c\Gamma_2) \simeq 0.17 \ll 1$, for one coupling atom. The correlation function of the cavity output can be measured in the same method as it is done experimentally, i.e., using one beam splitter and two avalanche photodiodes [13,16,69].

We notice that another alternative solid-state system to realize our Δ-configuration scheme can also be taken into account in the context of superconducting quantum circuits [81,82]. Such devices consist of a flux or transmon qutrit coupled to a coplanar waveguide resonator via the induced magnetic field, and have been implemented experimentally; see Ref. [82] for details.

IV. CALCULATION OF SECOND-ORDER PHOTON CORRELATION $g^{(2)}(0)$

In order to numerically solve the density matrix $\hat{\rho}$, we expand the state of the coupled atom-cavity system in the basis $|j, n\rangle = |j\rangle \otimes |n\rangle$, where $|j\rangle$ $(j = 1, 2, 3)$ is the state of the three-level atom and $|n\rangle$ is the Fock basis for the cavity mode with the photon number n $(n = 0, 1, 2, \ldots)$, as described before. The joint density operator $\hat{\rho}$ is a tensor product of the density matrix of the two subsystems and evolves in the time according to master equation (4). At the steady state, we set $\partial\hat{\rho}/\partial t = 0$ and truncate the Fock basis of the cavity mode. Once we achieve the density matrix $\hat{\rho}$, we can compute the mean value of any operator using $\langle\hat{\mathcal{O}}\rangle = \mathrm{Tr}(\hat{\mathcal{O}}\hat{\rho})$, where Tr denotes the trace. Here, we are particularly interested in the statistical properties of the cavity field, such as photon bunching and antibunching. The statistical properties of the transmitted photons can be measured by the normalized zero-time-delay second-order correlation function [83]

$$g^{(2)}(0) = \frac{\langle\hat{a}_c^{\dagger 2}\hat{a}_c^2\rangle}{\langle\hat{a}_c^{\dagger}\hat{a}_c\rangle^2} = \frac{\mathrm{Tr}(\hat{a}_c^{\dagger 2}\hat{a}_c^2\hat{\rho})}{[\mathrm{Tr}(\hat{a}_c^{\dagger}\hat{a}_c\hat{\rho})]^2}, \tag{5}$$

where, more concretely, the value of $g^{(2)}(0) < 1$ represents the photon antibunching (corresponding to sub-Poissonian photon statistics). It is a nonclassical effect of light and also is an important witness for the two-photon blockade effect which is used to characterize the quality of single-photon sources in applications. On the contrary, the value of $g^{(2)}(0) > 1$ denotes the photon bunching (super-Poissonian photon statistics), which is a classical effect. In particular, the value of $g^{(2)}(0) = 1$ is referred to as the coherent-state photon (Poissonian photon statistics), which is a quasiclassical effect.

V. NUMERICAL RESULTS AND DISCUSSIONS ABOUT CORRELATION $g^{(2)}(0)$

The second-order correlation function $g^{(2)}(0)$ is shown in Figs. 2(a)–2(d) as a function of the driving detuning $\delta/2\pi$ for four different atomic level configurations for the sake of an in-depth comparison. Specifically, this first simple configuration is to employ a standard two-level atom coupled to only a single-mode cavity field, which we refer to as a two-level configuration below. For the two-level configuration

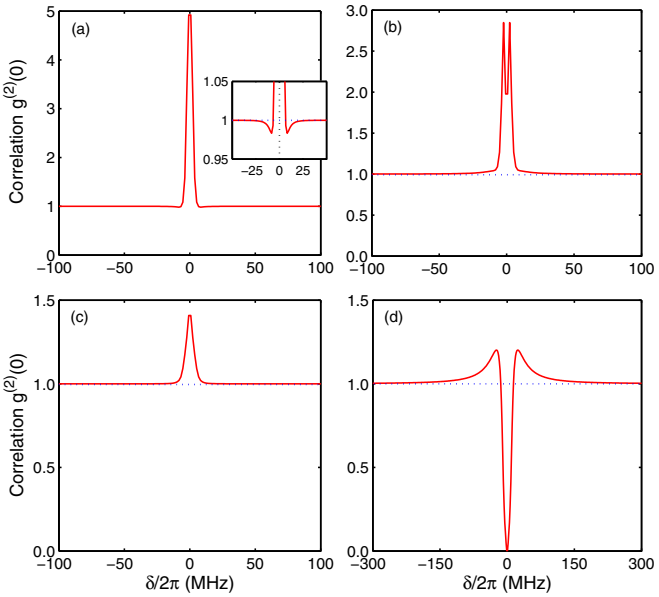

FIG. 2. Second-order correlation function $g^{(2)}(0)$ as a function of the driving detuning $\delta/2\pi$ for four different atomic configurations. (a) Standard two-level configuration, i.e., $g_c/2\pi = 4$ MHz, $\Omega_p/2\pi = 0$ MHz, and $\Omega_m/2\pi = 0$ MHz. The remaining parameters are chosen as $\kappa_c/2\pi = 8$ MHz, $\gamma_{21}/2\pi = 3$ MHz, $\eta/2\pi = 0.01$ MHz, and $\Delta_c/2\pi = 0$ MHz. Here, the inset is a zoomed-in view of both sides of the $g^{(2)}(0)$ spectrum around $\delta/2\pi = 0$ MHz. (b) Three-level Λ configuration: $g_c/2\pi = 4$ MHz, $\Omega_p/2\pi = 2$ MHz, and $\Omega_m/2\pi = 0$ MHz. The remaining parameters are chosen as $\kappa_c/2\pi = 8$ MHz, $\gamma_{21}/2\pi = 3$ MHz, $\gamma_{23}/2\pi = 3$ MHz, $\gamma_{31}/2\pi = 0.003$ MHz, $\eta/2\pi = 0.01$ MHz, $\Delta_c/2\pi = 0$ MHz, and $\Delta_p/2\pi = 0$ MHz. (c) Three-level V configuration: $g_c/2\pi = 4$ MHz, $\Omega_p/2\pi = 0$ MHz, and $\Omega_m/2\pi = 0.1$ MHz. The remaining parameters are chosen as $\kappa_c/2\pi = 8$ MHz, $\gamma_{21}/2\pi = 3$ MHz, $\gamma_{23}/2\pi = 3$ MHz, $\gamma_{31}/2\pi = 0.003$ MHz, $\eta/2\pi = 0.01$ MHz, $\Delta_c/2\pi = 0$ MHz, and $\Delta_m/2\pi = 0$ MHz. (d) Three-level Δ configuration: $g_c/2\pi = 4$ MHz, $\Omega_p/2\pi = 2$ MHz, and $\Omega_m/2\pi = 0.1$ MHz. The other parameters are chosen as $\kappa_c/2\pi = 8$ MHz, $\gamma_{21}/2\pi = 3$ MHz, $\gamma_{23}/2\pi = 3$ MHz, $\gamma_{31}/2\pi = 0.003$ MHz, $\eta/2\pi = 0.01$ MHz, $\Delta_c/2\pi = 0$ MHz, and $\Delta_p/2\pi = 0$ MHz. In (a)–(d), the blue dotted lines stand for $g^{(2)}(0) = 1$.

in Fig. 2(a), one can see that the form of $g^{(2)}(0)$ is symmetric with the strong photon bunching generating a maximum of $g^{(2)}(0) \simeq 4.9$ in the center $\delta/2\pi = 0$ MHz, and the weak photon antibunching generating a minimum dip of $g^{(2)}(0) \simeq 0.98$ at the driving detuning of $\delta/2\pi \simeq \pm 8$ MHz; see the inset of Fig. 2(a) for clarity. This weak photon antibunching in the two-level configuration can be explained according to the anharmonic nature of the ladder [6–10].

The second Λ configuration is used to introduce a three-level atom coupled to a pump field and a single-mode cavity field. For the three-level Λ configuration in Fig. 2(b), the profile of the second-order correlation function $g^{(2)}(0)$ takes on a peak-dip-peak structure due to the coupling of the pump field, where no antibunching can be seen for the whole range of driving detunings. The left- and right-side bunching peaks reach the same value of $g^{(2)}(0) \simeq 2.8$ at the driving detunings of $\delta \simeq \pm\Omega_p = \pm 2\pi \times 2$ MHz. The other central bunching dip corresponds to the value of $g^{(2)}(0) \simeq 1.9$ at the driving

detuning of $\delta/2\pi = 0$ MHz. Evidently, the distance between two side bunching peaks is proportional to the pump-field Rabi frequency. The physical mechanism behind this photon statistics behavior can be grasped by using the dressed-state picture, which can be obtained by solving the Hamiltonian of the three-level Λ configuration [6,7].

Effectively, a microwave field and a cavity field form a V configuration with a three-level atom. For the three-level V configuration in Fig. 2(c), a single peak in the $g^{(2)}(0)$ line shape distinctively appears at the resonance point $\delta/2\pi = 0$ MHz. For any detuning, there is no photon antibunching. This is due to the microwave-field coupling strength being less than the decay rates of the cavity field and the three-level atom. Note as well that the photon bunching is considerable for the certain detuning range $\delta/2\pi \in (-9.8, 9.8)$ MHz. At large detuning the photon statistics are those of a coherent state, with $g^{(2)}(0)$ equal to unity.

Finally, all the involved three fields (cavity, pump, and microwave) are switched on to simultaneously excite the three-level atom, which constitutes a Δ-type or cycle transition and closed-loop coupling. For brevity, we call it a three-level Δ configuration. With the help of this three-level Δ configuration in Fig. 2(d), we find that an obvious minimum and valley appear around the zero detuning, e.g., the minimum value of $g^{(2)}(0)$ reaches $g^{(2)}(0) = 0$ at $\delta/2\pi = 0$ MHz, in contrast to the cases of Figs. 2(a)–2(c). From Fig. 2(d), one can also observe that for the value of g_c falling in the weak-coupling regime, i.e., $g_c < (\kappa_c, \Gamma_2)$, strong antibunching $[g^{(2)}(0) = 0]$ can be realized. Like the previous schemes [30,31,33], this just falls into the regime of an unconventional single-photon blockade. Alternatively, the photon bunching is observed on both sides around $\delta/2\pi \simeq \pm 24.8$ MHz, where the values of $g^{(2)}(0)$ arrive at $g^{(2)}(0) \simeq 1.2$. The feature of the second-order correlation function $g^{(2)}(0)$ as shown in Fig. 2(d) for our Δ-configuration scheme is analogous to the case of a bimodal cavity with both of its modes coupled to a quantum dot [33].

Physically, for the three-level Δ configuration, this pronounced antibunching is because the quantum interference can happen between the two different two-photon excitation pathways as shown in Fig. 3(d): (i) directly inputting two photons in the cavity mode by the external driving, which we refer to as the direct pathway, i.e., $|1,0\rangle \xrightarrow{\eta} |1,1\rangle \xrightarrow{\sqrt{2}\eta} |1,2\rangle$, and (ii) the indirect pathway, i.e., $|1,0\rangle \xrightarrow{\Omega_m} |3,0\rangle \xrightarrow{\eta} |3,1\rangle \xrightarrow{\Omega_p} |2,1\rangle \xrightarrow{\sqrt{2}g_c} |1,2\rangle$, assisted by the pump and microwave fields. The photons coming from both pathways (i) and (ii) cannot occupy the two-photon state $|1,2\rangle$ owing to the interference of these two excitation pathways instead of the cavity-coupling cavity-induced quantum interference presented in previous works [30,31]. On the contrary, for the two-photon excitation pathways in a three-level Λ configuration, evidently the indirect excitation pathway (ii) in the transition part $|1,0\rangle \xrightarrow{\Omega_m} |3,0\rangle$ is cut off due to $\Omega_m = 0$ as shown in Fig. 3(b) and therefore no interference occurs. Similarly, for a three-level V configuration [see Fig. 3(c)], the transition part $|3,1\rangle \xrightarrow{\Omega_p} |2,1\rangle$ is switched off due to $\Omega_p = 0$. Overall, the transition pathways of four configurations shown in Fig. 3 are significantly different, leading to the rich line shapes of $g^{(2)}(0)$ in Fig. 2.

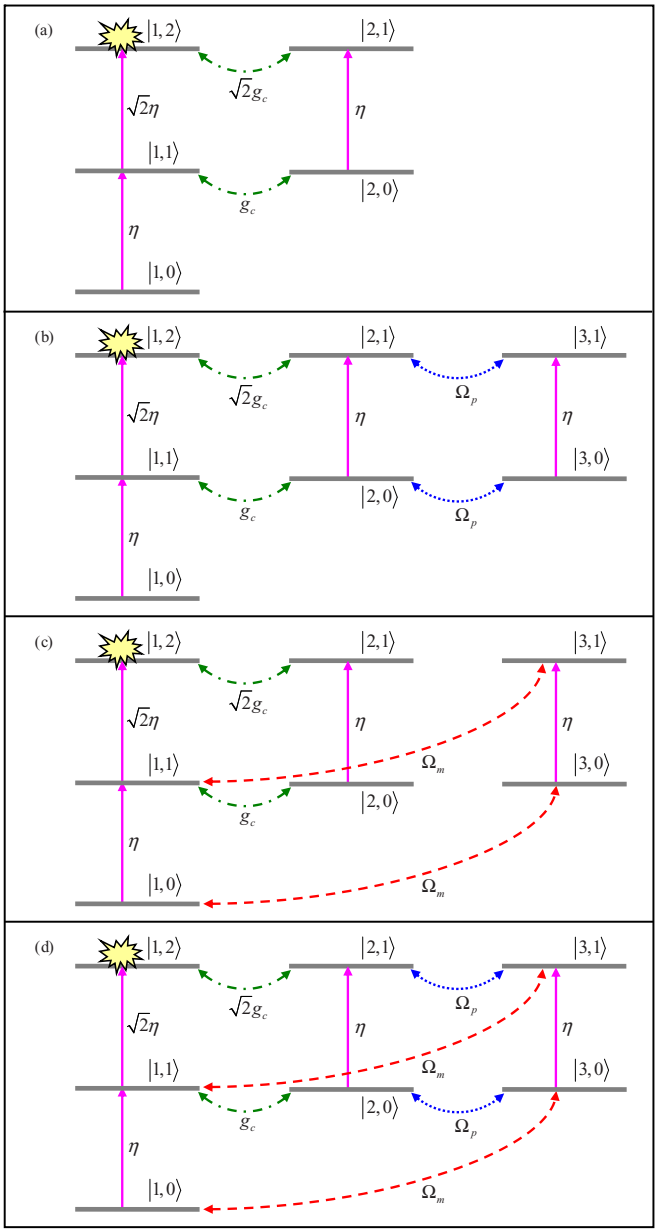

FIG. 3. Energy-level diagram showing the zero-, one-, and two-photon states (horizontal grey lines without arrows) and the transition pathways (color lines with arrows) for four different atomic configurations: (a) a standard two-level configuration, (b) a three-level Λ configuration, (c) a three-level V configuration, and (d) a three-level Δ configuration. States are labeled by $|j,n\rangle$ with the first number being the state of the three-level atom and the second number representing the Fock state for the cavity mode with the photon number n.

Alternatively, it is worthwhile to emphasize that, in general, when the pathway starting position is not the state $|1,0\rangle$ but the terminal position still is the state $|1,2\rangle$ in Fig. 3 for our considered single-cavity situation, the quantum interference of these excitation pathways does not play a role in the intensity correlation (i.e., the second-order correlation) and only plays a role in the amplitude correlation (the first-order correlation) [45]. Here, owing to the direct introduction of

the microwave driving field in the Δ system of Fig. 3(d) compared with the Λ system of Fig. 3(b), a new excitation pathway for the two-photon state obviously appears and thus forms a closed-loop transition structure; i.e., the interference starting point is the state $|1,0\rangle$ in Fig. 3 and the terminal point is the state $|1,2\rangle$ for the quantum interference of the excitation pathways leading to the two-photon state. This is just the principle difference between the Λ configuration of Fig. 3(b) and the Δ configuration of Fig. 3(d). In this scenario of the closed-loop pathway [see Fig. 3(d)], the well-behaved quantum interference can be efficiently achieved to generate the pronounced photon antibunching [see Fig. 2(d)].

We also can seek the time-dependent Schrödinger equation as an alternative way to provide the analytical description of the properties of the photon statistics like Refs. [41,45] in the scenario of a weak driving ($\eta \ll g_c, \kappa_c$), where a perturbative treatment is possible. According to Fig. 3(d), only the lower energy levels of the cavity mode are occupied and the solution of Eq. (4) can be approximated by $\hat{\rho} = |\psi(t)\rangle\langle\psi(t)|$ with the truncated state

$$|\psi(t)\rangle \simeq C_{10}|1,0\rangle + C_{11}|1,1\rangle + C_{12}|1,2\rangle + C_{20}|2,0\rangle + C_{21}|2,1\rangle + C_{30}|3,0\rangle + C_{31}|3,1\rangle, \tag{6}$$

where the state $|j,n\rangle$ is the same as the previous definition (cf. Sec. IV) and the coefficient C_{jn} represents the probability amplitude of the corresponding state $|j,n\rangle$. Based on the time-dependent Schrödinger equation $i\hbar\partial|\psi(t)\rangle/\partial t = \hat{H}'|\psi(t)\rangle$, where $\hat{H}' = \hat{H}_{\rm rot} - i\kappa_c\hat{a}_c^\dagger\hat{a}_c - i\Gamma_2\hat{\sigma}_{22}$ is the non-Hermitian Hamiltonian containing the optical cavity decay and three-level atomic damping terms in addition to the original Hamiltonian (3), the dynamics of the above coefficients C_{jn} are described by a set of coupled equations as follows:

$$i\frac{\partial C_{10}}{\partial t} = \Omega_m^* C_{30} + \eta^* C_{11}, \tag{7}$$

$$i\frac{\partial C_{11}}{\partial t} = (\delta - i\kappa_c)C_{11} + g_c^* C_{20} + \Omega_m^* C_{31} + \eta C_{10} + \sqrt{2}\eta^* C_{12}, \tag{8}$$

$$i\frac{\partial C_{12}}{\partial t} = 2(\delta - i\kappa_c)C_{12} + \sqrt{2}g_c^* C_{21} + \sqrt{2}\eta C_{11}, \tag{9}$$

$$i\frac{\partial C_{20}}{\partial t} = (\delta + \Delta_c - i\Gamma_2)C_{20} + g_c C_{11} + \Omega_p C_{30} + \eta^* C_{21}, \tag{10}$$

$$i\frac{\partial C_{21}}{\partial t} = (2\delta + \Delta_c - i\kappa_c - i\Gamma_2)C_{21} + \sqrt{2}g_c C_{12} + \Omega_p C_{31} + \eta C_{20}, \tag{11}$$

$$i\frac{\partial C_{30}}{\partial t} = (\delta + \Delta_c - \Delta_p)C_{30} + \Omega_p^* C_{20} + \Omega_m C_{10} + \eta^* C_{31}, \tag{12}$$

$$i\frac{\partial C_{31}}{\partial t} = (2\delta + \Delta_c - \Delta_p - i\kappa_c)C_{31} + \Omega_p^* C_{21} + \Omega_m C_{11} + \eta C_{30}. \tag{13}$$

In the steady state (i.e., $\partial C_{jn}/\partial t = 0$), we can obtain the following set of linear equations:

$$\Omega_m^* C_{30} + \eta^* C_{11} = 0, \tag{14}$$

$$(\delta - i\kappa_c)C_{11} + g_c^* C_{20} + \Omega_m^* C_{31} + \eta C_{10} + \sqrt{2}\eta^* C_{12} = 0, \tag{15}$$

$$2(\delta - i\kappa_c)C_{12} + \sqrt{2}g_c^* C_{21} + \sqrt{2}\eta C_{11} = 0, \tag{16}$$

$$(\delta + \Delta_c - i\Gamma_2)C_{20} + g_c C_{11} + \Omega_p C_{30} + \eta^* C_{21} = 0, \tag{17}$$

$$(2\delta + \Delta_c - i\kappa_c - i\Gamma_2)C_{21} + \sqrt{2}g_c C_{12} + \Omega_p C_{31} + \eta C_{20} = 0, \tag{18}$$

$$(\delta + \Delta_c - \Delta_p)C_{30} + \Omega_p^* C_{20} + \Omega_m C_{10} + \eta^* C_{31} = 0, \tag{19}$$

$$(2\delta + \Delta_c - \Delta_p - i\kappa_c)C_{31} + \Omega_p^* C_{21} + \Omega_m C_{11} + \eta C_{30} = 0. \tag{20}$$

In the limit of weak driving, we have the relationship $C_{10} \gg C_{11}, C_{20}, C_{30} \gg C_{12}, C_{21}, C_{31}$. In this circumstance, the normalized zero-time-delay second-order correlation function (5) can be reexpressed in terms of the coefficients C_{jn} as

$$g^{(2)}(0) = \frac{\sum_{j,n} n(n-1)|C_{jn}|^2}{\left(\sum_{j,n} n|C_{jn}|^2\right)^2} \simeq \frac{2|C_{12}|^2}{|C_{11}|^4}, \tag{21}$$

where the sum indices are $j = 1, 2, 3$ and $n = 0, 1, 2, \ldots$. The coefficients C_{12} and C_{11} can be determined by directly solving the set of coupled algebraic equations (14)–(20). The calculated results are in agreement with those in Fig. 2. Nevertheless, the analytical expressions of the second-order correlation function $g^{(2)}(0)$ or the conditions for $g^{(2)}(0) \to 0$ or $C_{12} \simeq 0$ (strong photon antibunching) are too long and bulky to be included here. From the derivations mentioned above, we can see that $g^{(2)}(0)$ is closely related to both the pump and microwave fields (Ω_p and Ω_m), playing an important role in generating strong antibunching for a three-level Δ configuration. In the following, we focus on the situation with such a well-behaved three-level Δ configuration.

In Fig. 4, we show the transmission through the cavity corresponding to the three-level Δ configuration used in Fig. 2(d). As can be seen in this figure, the transmission reaches the maximum value in the center, $\delta/2\pi = 0\,\text{MHz}$, where the second-order correlation function $g^{(2)}(0) = 0$. This high transmission and low $g^{(2)}(0)$ are useful for the correlation measurement [84] and are also interesting for designing a practical experiment.

In order to give a better insight into the effect of the pump and microwave fields (Ω_p and Ω_m) on the photon statistics of the single-mode cavity field in the three-level Δ configuration, the second-order correlation function $g^{(2)}(0)$ is displayed in Figs. 5(a) and 5(b). Figure 5(a) presents the color-scale two-dimensional (2D) map of $g^{(2)}(0)$ as a function of the driving detuning $\delta/2\pi$ and the pump-field Rabi frequency $\Omega_p/2\pi$. The color bar on the right-hand side represents the magnitude of $g^{(2)}(0)$. In looking at the results in Fig. 5(a), we find that the line shape of the second-order correlation function $g^{(2)}(0)$

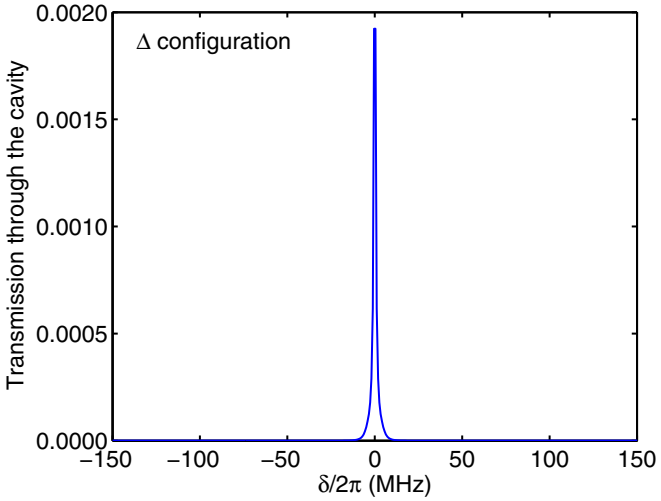

FIG. 4. The transmission through the cavity corresponding to the three-level Δ configuration used in Fig. 2(d). The system parameters are the same as in Fig. 2(d).

under the change of the pump-field Rabi frequency $\Omega_p/2\pi$ is always symmetric with respect to the driving detuning $\delta/2\pi = 0\,\mathrm{MHz}$, which exhibits the single deep antibunching dip and the double bunching peaks. On the one hand, for the central antibunching dip at the driving frequency $\delta/2\pi = 0\,\mathrm{MHz}$, the value of $g^{(2)}(0)$ can reach and maintain $g^{(2)}(0) = 0$ when varying $\Omega_p/2\pi$. On the other hand, for the two bunching peaks located on both sides, the degree of the photon bunching is gradually enhanced with the increasing of $\Omega_p/2\pi$ and the separation of the two bunching peaks is gradually enlarged along the abscissa axis. Figure 5(b) show the color-scale 2D map of $g^{(2)}(0)$ versus the driving detuning $\delta/2\pi$ and the

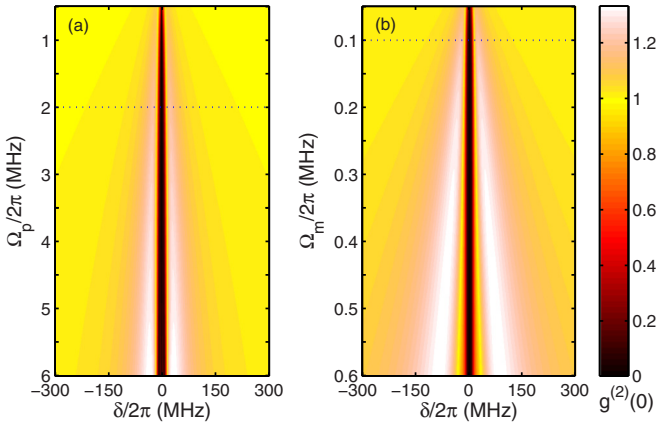

FIG. 5. Contour plots of second-order correlation function $g^{(2)}(0)$ versus (a) the driving detuning $\delta/2\pi$ and the pump-field Rabi frequency $\Omega_p/2\pi$ as well as (b) the driving detuning $\delta/2\pi$ and the microwave-field Larmor frequency $\Omega_m/2\pi$ for the three-level Δ configuration. In (a), we take $\Omega_m/2\pi = 0.1\,\mathrm{MHz}$, whereas in (b), $\Omega_p/2\pi = 2\,\mathrm{MHz}$. In both (a) and (b), the black dotted lines correspond to $\Omega_p/2\pi = 2\,\mathrm{MHz}$ and $\Omega_m/2\pi = 0.1\,\mathrm{MHz}$. The common parameters are chosen as $g_c/2\pi = 4\,\mathrm{MHz}$, $\kappa_c/2\pi = 8\,\mathrm{MHz}$, $\gamma_{21}/2\pi = 3\,\mathrm{MHz}$, $\gamma_{23}/2\pi = 3\,\mathrm{MHz}$, $\gamma_{31}/2\pi = 0.003\,\mathrm{MHz}$, $\eta/2\pi = 0.01\,\mathrm{MHz}$, $\Delta_c/2\pi = 0\,\mathrm{MHz}$, and $\Delta_p/2\pi = 0\,\mathrm{MHz}$.

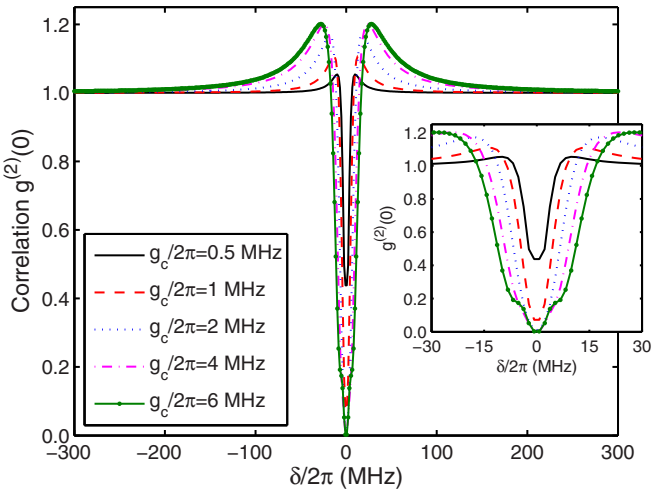

FIG. 6. Second-order correlation function $g^{(2)}(0)$ as a function of the driving detuning $\delta/2\pi$ for five different values of the atom-cavity coupling constant g_c in the three-level Δ configuration. The inset shows an enlarged view of $g^{(2)}(0)$ near $\delta/2\pi = 0\,\mathrm{MHz}$. The other parameters are chosen as $g_c/2\pi = 4\,\mathrm{MHz}$, $\Omega_p/2\pi = 2\,\mathrm{MHz}$, $\Omega_m/2\pi = 0.1\,\mathrm{MHz}$, $\kappa_c/2\pi = 8\,\mathrm{MHz}$, $\gamma_{21}/2\pi = 3\,\mathrm{MHz}$, $\gamma_{23}/2\pi = 3\,\mathrm{MHz}$, $\gamma_{31}/2\pi = 0.003\,\mathrm{MHz}$, $\eta/2\pi = 0.01\,\mathrm{MHz}$, $\Delta_c/2\pi = 0\,\mathrm{MHz}$, and $\Delta_p/2\pi = 0\,\mathrm{MHz}$.

microwave-field Larmor frequency $\Omega_m/2\pi$. As can be seen in Fig. 5(b), the evolution of $g^{(2)}(0)$ with increasing $\Omega_m/2\pi$ is analogous to that of Fig. 5(a). Based on the above analysis, we can conclude that there is no strict requirement for the strengths of the pump and microwave fields in generating the strong photon antibunching $[g^{(2)}(0) = 0]$ in the three-level Δ configuration.

We now investigate how the statistical property of the single-mode cavity field is modified by the atom-cavity coupling constant $g_c/2\pi$ by plotting the second-order correlation function $g^{(2)}(0)$ in Fig. 6. From these plots, one can see that (i) there exists a minimum value of $g^{(2)}(0)$ at the driving detuning $\delta/2\pi = 0\,\mathrm{MHz}$; (ii) the minimum value of $g^{(2)}(0)$ rapidly decreases with increasing the atom-cavity coupling constant $g_c/2\pi$ gradually and the degree of the photon antibunching quickly increases; and (iii) the minimum value of $g^{(2)}(0)$ reaches zero and tends to saturate when $g_c/2\pi \geqslant 2\,\mathrm{MHz}$. This result clearly illustrates that a strong photon antibunching $[g^{(2)}(0) = 0]$ with sub-Poissonian quantum statistics for the cavity field output can be well achieved in the weak-coupling regime, for example, with the values of considered parameters being $g_c/2\pi = 2\,\mathrm{MHz}$, $\kappa_c/2\pi = 8\,\mathrm{MHz}$, and $\Gamma_2/2\pi = 6\,\mathrm{MHz}$. The weak-coupling condition is beneficial because it allows the use of low-finesse cavities which are readily available in many cavity-QED systems.

VI. CONCLUSIONS

In summary, we have demonstrated a feasible experimental scheme for realizing strong photon antibunching by utilizing a three-level atom weakly coupled to a single-mode optical cavity, a pump field in free space, and a microwave field. Both the involved three fields (cavity, pump, and

microwave) and the driven three-level atom thus constitute the Δ-type transition and closed-loop coupling, i.e., the so-called three-level Δ configuration. When switching off either of the pump and microwave fields, we recover a three-level Λ or V configuration. When switching off both the pump and microwave fields, we obtain a two-level configuration. Based on experimentally realistic atom-cavity parameters, for four configurations we evaluate the steady-state second-order correlation functions $g^{(2)}(0)$ of the quantized cavity field and further identify these four different configurations with the quality of the photon antibunching. It is found that the quality of the photon antibunching in the three-level Δ configuration can be significantly improved, as compared to the other three configurations. The complete photon blockade corresponding to the value of $g^{(2)}(0) = 0$ can be generated without detuning the driving and cavity resonance in such a three-level Δ configuration. Moreover, this strong photon antibunching effect can appear in the weak-coupling regime of light-atom interactions. Therefore, the constraint condition on the strong coupling in the coupled atom-field system is unnecessary. We attribute these features to the formation of the quantum interference between the two transition paths from the three-level Δ-type atom weakly coupled to the cavity, pump, and microwave fields. We also discuss the experimental feasibility of the proposed scheme using current state-of-the-art atom-cavity architecture. The obtained results offer us more detailed insights into the underlying mechanism behind photon antibunching in the closed-loop coupling and may have potential application in the single-photon generation.

ACKNOWLEDGMENTS

We would like to express our sincere appreciation to the two referees for their valuable comments and suggestions, which significantly improved the paper. We gratefully acknowledge the fruitful discussions with Xiaoxue Yang and Rong Yu during the manuscript preparation. J.L. is supported in part by the National Natural Science Foundation of China through Grant No. 11675058 and by the Fundamental Research Funds for the Central Universities (Huazhong University of Science and Technology) under Project No. 2018KFYYXJJ037. C.D. is supported in part by the National Natural Science Foundation of China through Grants No. 11705131 and No. U1504111, as well as by the Science Research Funds of Wuhan Institute of Technology under Project No. K201744. Y.W. is supported in part by the National Key Research and Development Program of China under Contract No. 2016YFA0301200 as well as by the National Natural Science Foundation of China through Grants No. 11875029 and No. 11574104.

[1] E. M. Purcell, Spontaneous emission probabilities at radio frequencies, Phys. Rev. **69**, 681 (1946).

[2] J. M. Gérard, B. Sermage, B. Gayral, B. Legrand, E. Costard, and V. Thierry-Mieg, Enhanced Spontaneous Emission by Quantum Boxes in a Monolithic Optical Microcavity, Phys. Rev. Lett. **81**, 1110 (1998).

[3] M. Brune, F. Schmidt-Kaler, A. Maali, J. Dreyer, E. Hagley, J. M. Raimond, and S. Haroche, Quantum Rabi Oscillation: A Direct Test of Field Quantization in a Cavity, Phys. Rev. Lett. **76**, 1800 (1996).

[4] R. J. Thompson, G. Rempe, and H. J. Kimble, Observation of Normal-Mode Splitting for an Atom in an Optical Cavity, Phys. Rev. Lett. **68**, 1132 (1992).

[5] T. Yoshie, A. Scherer, J. Hendrickson, G. Khitrova, H. M. Gibbs, G. Rupper, C. Ell, O. B. Shchekin, and D. G. Deppe, Vacuum Rabi splitting with a single quantum dot in a photonic crystal nanocavity, Nature (London) **432**, 200 (2004).

[6] M. O. Scully and M. S. Zubairy, *Quantum Optics* (Cambridge University Press, Cambridge, UK, 1997).

[7] G. S. Agarwal, *Quantum Optics* (Cambridge University Press, Cambridge, UK, 2013).

[8] J. M. Fink, M. Göppl, M. Baur, R. Bianchetti, P. J. Leek, A. Blais, and A. Wallraff, Climbing the Jaynes-Cummings ladder and observing its $\sqrt{n}$ nonlinearity in a cavity QED system, Nature (London) **454**, 315 (2008).

[9] J. Kasprzak, S. Reitzenstein, E. A. Muljarov, C. Kistner, C. Schneider, M. Strauss, S. Höling, A. Forchel, and W. Langbein, Up on the Jaynes-Cummings ladder of a quantum-dot/microcavity system, Nat. Mater. **9**, 304 (2010).

[10] J. Vučković, Quantum optics and cavity QED with quantum dots in photonic crystals, in *Quantum Optics and Nanophotonics*, edited by C. Fabre, V. Sandoghdar, N. Treps, and L. F. Cugliandolo (Oxford University Press, Oxford, 2017), pp. 365–406.

[11] F. P. Laussy, E. del Valle, M. Schrapp, A. Laucht, and J. J. Finley, Climbing the Jaynes-Cummings ladder by photon counting, J. Nanophotonics **6**, 061803 (2012).

[12] A. Imamoğlu, H. Schmidt, G. Woods, and M. Deutsch, Strongly Interacting Photons in a Nonlinear Cavity, Phys. Rev. Lett. **79**, 1467 (1997).

[13] K. M. Birnbaum, A. Boca, R. Miller, A. D. Boozer, T. E. Northup, and H. J. Kimble, Photon blockade in an optical cavity with one trapped atom, Nature (London) **436**, 87 (2005).

[14] B. Dayan, A. S. Parkins, T. Aoki, E. P. Ostby, K. J. Vahala, and H. J. Kimble, A photon turnstile dynamically regulated by one atom, Science **319**, 1062 (2008).

[15] W.-W. Deng, G.-X. Li, and H. Qin, Enhancement of the two-photon blockade in a strong-coupling qubit-cavity system, Phys. Rev. A **91**, 043831 (2015).

[16] C. Hamsen, K. N. Tolazzi, T. Wilk, and G. Rempe, Two-Photon Blockade in an Atom-Driven Cavity QED System, Phys. Rev. Lett. **118**, 133604 (2017).

[17] A. Faraon, I. Fushman, D. Englund, N. Stoltz, P. Petroff, and J. Vučković, Coherent generation of non-classical light on a chip via photon-induced tunnelling and blockade, Nat. Phys. **4**, 859 (2008).

[18] A. Reinhard, T. Volz, M. Winger, A. Badolato, K. J. Hennessy, E. L. Hu, and A. Imamoğlu, Strongly correlated photons on a chip, Nat. Photonics **6**, 93 (2012).

[19] K. Müller, A. Rundquist, K. A. Fischer, T. Sarmiento, K. G. Lagoudakis, Y. A. Kelaita, C. S. Muñoz, E. del Valle, F. P. Laussy, and J. Vučković, Coherent Generation of Nonclassical Light on Chip via Detuned Photon Blockade, Phys. Rev. Lett. **114**, 233601 (2015).

[20] M. Radulaski, K. A. Fischer, and J. Vučković, Nonclassical light generation from III-V and group-IV solid-state cavity quantum systems, in *Advances in Atomic, Molecular, and Optical Physics* (Academic Press, New York, 2017), Vol. 66, pp. 111–179.

[21] O. Gazzano, S. Michaelis de Vasconcellos, C. Arnold, A. Nowak, E. Galopin, I. Sagnes, L. Lanco, A. Lemaître, and P. Senellart, Bright solid-state sources of indistinguishable single photons, Nat. Commun. **4**, 1425 (2013).

[22] L. D. Santis, C. Antón, B. Reznychenko, N. Somaschi, G. Coppola, J. Senellart, C. Gómez, A. Lemaître, I. Sagnes, A. G. White, L. Lanco, A. Auffèves, and P. Senellart, A solid-state single-photon filter, Nat. Nanotechnol. **12**, 663 (2017).

[23] E. Illes and S. Hughes, Photon antibunching in strongly coupled exciton-semiconductor cavity systems: Role of off-resonant coupling to multiple excitons, Phys. Rev. B **81**, 121310(R) (2010).

[24] Y.-M. He, Y. He, Y.-J. Wei, D. Wu, M. Atatüre, C. Schneider, S. Höfling, M. Kamp, C.-Y. Lu, and J.-W. Pan, On-demand semiconductor single-photon source with near-unity indistinguishability, Nat. Nanotechnol. **8**, 213 (2013).

[25] A. J. Hoffman, S. J. Srinivasan, S. Schmidt, L. Spietz, J. Aumentado, H. E. Türeci, and A. A. Houck, Dispersive Photon Blockade in a Superconducting Circuit, Phys. Rev. Lett. **107**, 053602 (2011).

[26] C. Lang, D. Bozyigit, C. Eichler, L. Steffen, J. M. Fink, A. A. Abdumalikov, M. Baur, S. Filipp, M. P. da Silva, A. Blais, and A. Wallraff, Observation of Resonant Photon Blockade at Microwave Frequencies Using Correlation Function Measurements, Phys. Rev. Lett. **106**, 243601 (2011).

[27] Y.-x. Liu, X.-W. Xu, A. Miranowicz, and F. Nori, From blockade to transparency: Controllable photon transmission through a circuit-QED system, Phys. Rev. A **89**, 043818 (2014).

[28] R. Huang, A. Miranowicz, J.-Q. Liao, F. Nori, and H. Jing, Nonreciprocal Photon Blockade, Phys. Rev. Lett. **121**, 153601 (2018); B. Li, R. Huang, X.-W. Xu, A. Miranowicz, and H. Jing, Nonreciprocal unconventional photon blockade, Photonics Res. **7**, 630 (2019).

[29] Y. H. Zhou, H. Z. Shen, X. Y. Zhang, and X. X. Yi, Zero eigenvalues of a photon blockade induced by a non-Hermitian Hamiltonian with a gain cavity, Phys. Rev. A **97**, 043819 (2018).

[30] T. C. H. Liew and V. Savona, Single Photons from Coupled Quantum Modes, Phys. Rev. Lett. **104**, 183601 (2010).

[31] M. Bamba, A. Imamoğlu, I. Carusotto, and C. Ciuti, Origin of strong photon antibunching in weakly nonlinear photonic molecules, Phys. Rev. A **83**, 021802(R) (2011).

[32] M.-A. Lemonde, N. Didier, and A. A. Clerk, Antibunching and unconventional photon blockade with Gaussian squeezed states, Phys. Rev. A **90**, 063824 (2014).

[33] A. Majumdar, M. Bajcsy, A. Rundquist, and J. Vučković, Loss-Enabled Sub-Poissonian Light Generation in a Bimodal Nanocavity, Phys. Rev. Lett. **108**, 183601 (2012).

[34] T. Shi and S. Fan, Two-photon transport through a waveguide coupling to a whispering-gallery resonator containing an atom and photon-blockade effect, Phys. Rev. A **87**, 063818 (2013).

[35] W. Zhang, Z. Y. Yu, Y. M. Liu, and Y. W. Peng, Optimal photon antibunching in a quantum-dot-bimodal-cavity system, Phys. Rev. A **89**, 043832 (2014).

[36] M. Bradford and J.-T. Shen, Architecture dependence of photon antibunching in cavity quantum electrodynamics, Phys. Rev. A **92**, 023810 (2015).

[37] Y. L. Liu, G. Z. Wang, Y.-x. Liu, and F. Nori, Mode coupling and photon antibunching in a bimodal cavity containing a dipole quantum emitter, Phys. Rev. A **93**, 013856 (2016).

[38] J. Li and Y. Wu, Quality of photon antibunching in two cavity-waveguide arrangements on a chip, Phys. Rev. A **98**, 053801 (2018).

[39] C. Wang, Y.-L. Liu, R. Wu, and Y.-x. Liu, Phase-modulated photon antibunching in a two-level system coupled to two cavities, Phys. Rev. A **96**, 013818 (2017).

[40] A. Majumdar and D. Gerace, Single-photon blockade in doubly resonant nanocavities with second-order nonlinearity, Phys. Rev. B **87**, 235319 (2013).

[41] H. Flayac and V. Savona, Input-output theory of the unconventional photon blockade, Phys. Rev. A **88**, 033836 (2013).

[42] S. Ferretti, V. Savona, and D. Gerace, Optimal antibunching in passive photonic devices based on coupled nonlinear resonators, New J. Phys. **15**, 025012 (2013).

[43] D. Gerace and V. Savona, Unconventional photon blockade in doubly resonant microcavities with second-order nonlinearity, Phys. Rev. A **89**, 031803(R) (2014).

[44] H. Flayac, D. Gerace, and V. Savona, An all-silicon single-photon source by unconventional photon blockade, Sci. Rep. **5**, 11223 (2015).

[45] H. Flayac and V. Savona, Unconventional photon blockade, Phys. Rev. A **96**, 053810 (2017).

[46] X.-W. Xu and Y. Li, Tunable photon statistics in weakly nonlinear photonic molecules, Phys. Rev. A **90**, 043822 (2014).

[47] H. Z. Shen, Y. H. Zhou, and X. X. Yi, Tunable photon blockade in coupled semiconductor cavities, Phys. Rev. A **91**, 063808 (2015); Y. H. Zhou, H. Z. Shen, and X. X. Yi, Unconventional photon blockade with second-order nonlinearity, *ibid.* **92**, 023838 (2015).

[48] H. Flayac and V. Savona, Single photons from dissipation in coupled cavities, Phys. Rev. A **94**, 013815 (2016).

[49] V. Savona, Unconventional photon blockade in coupled optomechanical systems, arXiv:1302.5937.

[50] X.-W. Xu and Y. J. Li, Antibunching photons in a cavity coupled to an optomechanical system, J. Phys. B: At. Mol. Phys. **46**, 035502 (2013).

[51] A. Miranowicz, J. Bajer, N. Lambert, Y.-x. Liu, and F. Nori, Tunable multiphonon blockade in coupled nanomechanical resonators, Phys. Rev. A **93**, 013808 (2016).

[52] B. Sarma and A. K. Sarma, Unconventional photon blockade in three-mode optomechanics, Phys. Rev. A **98**, 013826 (2018).

[53] L.-L. Zheng, T.-S. Yin, Qian Bin, X.-Y. Lü, and Ying Wu, Single-photon-induced phonon blockade in a hybrid spin-optomechanical system, Phys. Rev. A **99**, 013804 (2019).

[54] M. Bamba and C. Ciuti, Counter-polarized single-photon generation from the auxiliary cavity of a weakly nonlinear photonic molecule, Appl. Phys. Lett. **99**, 171111 (2011).

[55] O. Kyriienko, I. A. Shelykh, and T. C. H. Liew, Tunable single-photon emission from dipolaritons, Phys. Rev. A **90**, 033807 (2014).

[56] J. C. López Carreño, C. Sánchez Muñoz, D. Sanvitto, E. del Valle, and F. P. Laussy, Exciting Polaritons with Quantum Light, Phys. Rev. Lett. **115**, 196402 (2015).

[57] H. J. Snijders, J. A. Frey, J. Norman, H. Flayac, V. Savona, A. C. Gossard, J. E. Bowers, M. P. van Exter, D. Bouwmeester, and W. Löffler, Observation of the Unconventional Photon Blockade, Phys. Rev. Lett. **121**, 043601 (2018).

[58] C. Vaneph, A. Morvan, G. Aiello, M. Féchant, M. Aprili, J. Gabelli, and J. Estève, Observation of the Unconventional Photon Blockade Effect in the Microwave Domain, Phys. Rev. Lett. **121**, 043602 (2018).

[59] M. Fleischhauer, A. Imamoglu, and J. P. Marangos, Electromagnetically induced transparency: Optics in coherent media, Rev. Mod. Phys. **77**, 633 (2005).

[60] M. Bienert and G. Morigi, Cavity cooling of a trapped atom using electromagnetically induced transparency, New J. Phys. **14**, 023002 (2012).

[61] J. A. Souza, E. Figueroa, H. Chibani, C. J. Villas-Boas, and G. Rempe, Coherent Control of Quantum Fluctuations Using Cavity Electromagnetically Induced Transparency, Phys. Rev. Lett. **111**, 113602 (2013).

[62] T. Kampschulte, W. Alt, S. Manz, M. Martinez-Dorantes, R. Reimann, S. Yoon, D. Meschede, M. Bienert, and G. Morigi, Electromagnetically-induced-transparency control of single-atom motion in an optical cavity, Phys. Rev. A **89**, 033404 (2014).

[63] H. S. Borges and C. J. Villas-Bôas, Quantum PHASE gate based on electromagnetically induced transparency in optical cavities, Phys. Rev. A **94**, 052337 (2016).

[64] J. Sheng, Y. Chao, S. Kumar, H. Fan, J. Sedlacek, and J. P. Shaffer, Intracavity Rydberg-atom electromagnetically induced transparency using a high-finesse optical cavity, Phys. Rev. A **96**, 033813 (2017).

[65] C. Hamsen, K. N. Tolazzi, T. Wilk, and G. Rempe, Strong coupling between photons of two light fields mediated by one atom, Nat. Phys. **14**, 885 (2018).

[66] R. R. Oliveira, H. S. Borges, J. A. Souza, and C. J. Villas-Bôas, Quantum memory and optical transistor based on electromagnetically induced transparency in optical cavities, arXiv:1603.05127.

[67] C. Gardiner and P. Zoller, *Quantum Noise: A Handbook of Markovian and Non-Markovian Quantum Stochastic Methods with Applications to Quantum Optics* (Springer, Berlin, 2004).

[68] D. A. Steck, Rubidium ^{87}Rb *D* line data, http://steck.us/alkalidata/rubidium87numbers.pdf

[69] M. Mücke, J. Bochmann, C. Hahn, A. Neuzner, C. Nölleke, A. Reiserer, G. Rempe, and S. Ritter, Generation of single photons from an atom-cavity system, Phys. Rev. A **87**, 063805 (2013).

[70] M. Mücke, E. Figueroa, J. Bochmann, C. Hahn, K. Murr, S. Ritter, C. J. Villas-Boas, and G. Rempe, Electromagnetically induced transparency with single atoms in a cavity, Nature (London) **465**, 755 (2010).

[71] R. Reimann, Ph.D. thesis, Institut für Angewandte Physik, Universität Bonn, 2014, https://hss.ulb.uni-bonn.de/2014/3832/3832.pdf

[72] J. McKeever, A. Boca, A. D. Boozer, R. Miller, J. R. Buck, A. Kuzmich, and H. J. Kimble, Deterministic generation of single photons from one atom trapped in a cavity, Science **303**, 1992 (2004).

[73] T. Wilk, S. C. Webster, A. Kuhn, and G. Rempe, Single-atom single-photon quantum interface, Science **317**, 488 (2007).

[74] I. Schuster, A. Kubanek, A. Fuhrmanek, T. Puppe, P. W. H. Pinkse, K. Murr, and G. Rempe, Nonlinear spectroscopy of photons bound to one atom, Nat. Phys. **4**, 382 (2008).

[75] A. Reiserer, N. Kalb, G. Rempe, and S. Ritter, A quantum gate between a flying optical photon and a single trapped atom, Nature (London) **508**, 237 (2014).

[76] A. Reiserer and G. Rempe, Cavity-based quantum networks with single atoms and optical photons, Rev. Mod. Phys. **87**, 1379 (2015).

[77] B. Hacker, S. Welte, G. Rempe, and S. Ritter, A photon-photon quantum gate based on a single atom in an optical resonator, Nature (London) **536**, 193 (2016).

[78] M. Körber, O. Morin, S. Langenfeld, A. Neuzner, S. Ritter, and G. Rempe, Decoherence-protected memory for a single-photon qubit, Nat. Photonics **12**, 18 (2018).

[79] B. Hacker, S. Welte, S. Daiss, A. Shaukat, S. Ritter, L. Li, and G. Rempe, Deterministic creation of entangled atom-light Schrödinger-cat states, Nat. Photonics **13**, 110 (2019).

[80] J. Han, T. Vogt, C. Gross, D. Jaksch, M. Kiffner, and W. Li, Coherent Microwave-to-Optical Conversion via Six-Wave Mixing in Rydberg Atoms, Phys. Rev. Lett. **120**, 093201 (2018).

[81] J. Q. You and F. Nori, Atomic physics and quantum optics using superconducting circuits, Nature (London) **474**, 589 (2011).

[82] X. Gu, A. F. Kockum, A. Miranowicz, Y.-x. Liu, and F. Nori, Microwave photonics with superconducting quantum circuits, Phys. Rep. **718-719**, 1 (2017).

[83] R. Loudon, *The Quantum Theory of Light* (Oxford University Press, Oxford, UK, 2003).

[84] T. Peyronel, O. Firstenberg, Q.-Y. Liang, S. Hofferberth, A. V. Gorshkov, T. Pohl, M. D. Lukin, and V. Vuletić, Quantum nonlinear optics with single photons enabled by strongly interacting atoms, Nature (London) **488**, 57 (2012).